

ARCHITECTING A COMMUNICATION SATELLITE PRODUCT LINE

Rania Hassan* Olivier de Weck† Philip Springmann‡

Massachusetts Institute of Technology
 77 Massachusetts Ave, Cambridge, MA 02139

ABSTRACT

Current unfavorable market conditions have shifted the preference of commercial communication satellite operators from large spacecraft systems with high bandwidth capacities, to small and medium size spacecraft. However, most satellite manufacturers have not caught up yet with this trend and are still positioned as providers of large capacity satellite systems. This paper investigates the application of product family concepts to the design of commercial satellites in an effort to formulate an approach that allows a manufacturer to develop a series of satellites with varying sizes based on similar architectures. Applying product family concepts could allow satellite manufacturers to lower cost, shorten development cycles, and reduce market risk by catering to a number of market segments. This paper formulates the satellite product line design problem into a multiobjective optimization problem that characterizes the tradeoffs and resolves the tension between product line commonalities and the performance of each of the product line individual satellites. This research couples a Genetic Algorithm (GA), which is an evolutionary global search method that mimics the behavior of biological populations, with a satellite sizing model to find optimal product lines with common technology choices. The preliminary results demonstrate the effectiveness of the multiobjective optimization approach in applying product family concepts to the design of commercial communication satellites.

NOMENCLATURE

A_{SA}	solar array area
$A_{radiator}$	thermal radiator area
c	penalty multiplier
$C_{battery}$	battery capacity
$d_{radiator}$	thermal radiator depth

DF	cells performance degradation factor
e	surface emissivity
f	fitness function
f_{OBO}	3 dB output back-off power scaling factor
g	inequality constraint function
$H_{radiator}$	thermal radiator height
HPA_{OBO}	number of high power amplifiers at 3 dB output back-off power
HPA_{active}	total number of active high power amplifiers in each coverage area
$HPA_{redundant}$	number of redundant high power amplifiers
I_{sp}	specific impulse
L_d	diode loss
L_{SA}	deployed length of solar array
M	number of active components
$M_{()}$	mass of
N	number of available components
N_{obj}	number of objective functions
N_{GaAs}	number of gallium arsenide panels
N_{Si}	number of silicon panels
$N_{battery\ cells}$	number of battery cells
P_{DC}	high power amplifier input DC power
P_{RF}	amplifier output RF power
$P_{cellBOL}$	solar cell beginning of life power
$P_{cellEOL}$	solar cell end of life power
$P_{()}$	power of
\dot{Q}	dissipated heat flow rate
$R_{()}$	reliability of
s	Stefan-Boltzmann constant
SF	scaling factor
T_{SH}	outer sink hot temperature

* Postdoctoral Associate, Engineering Systems and Aeronautics & Astronautics, rhassan@mit.edu, Member AIAA.

† Assistant Professor, Aeronautics & Astronautics and Engineering Systems, deweck@mit.edu, Senior Member AIAA.

‡ Undergraduate Student, Aeronautics and Astronautics, pspringm@mit.edu, Student Member AIAA.

Copyright © 2004 by R. Hassan. Published by AIAA, with permission.

$T_{eclipse}$	maximum eclipse time
$T_{radiator}$	radiator maximum temperature
V_d	voltage per battery cell
$W_{N/S}$	spacecraft North/South panel width
\mathbf{X}	design variable vector
ΔV	change (“delta”) in velocity
Φ	vector of objectives
ϕ	objective function
η_{EPC}	electric power conditioning efficiency
η_{HPA}	high power amplifier efficiency
$\eta_{thruster}$	thruster efficiency
λ	failure rate
$\rho_{radiator}$	radiator material density
\forall_i	for all i
\exists_i	there exists (at least) one i

INTRODUCTION

This research is an extension of the doctoral work of the first author in which optimization approaches were developed and investigated for the design of single spacecraft systems.¹ This doctoral work included reliability-based spacecraft design using both multiobjective optimization approaches² and probabilistic design approaches³. However, the present paper adds an original contribution to the design process of commercial communication satellites, which is the issue of designing for architecture modularity and platform commonalities using optimization approaches. The next few paragraphs will introduce the concept of “platforming” or designing product families and will present a brief literature review of the topic.

Platforming strategies allow for the development of product families whose individual members must be optimized to survive market competition within their respective market segments, but also must share features, components, subsystems, and processes to minimize development costs to the manufacturer. To resolve the tension between these usually conflicting objectives, i.e. the objective of optimizing the performance of individual products and the objective of maximizing the commonalities between product family members, few researchers have applied optimization approaches. Applications of these approaches include: an automotive product line⁴, a family of blended-wing-body (BWB) passenger airplanes⁵, a family of general aviation aircraft⁶, and a family of deep space exploration missions⁷. The application of product family concepts to spacecraft design is especially difficult because it involves very large investments, low

production levels, and long development cycles. Caffery et al. summarize these strategic⁸, economic⁹ and technical¹⁰ hurdles with a focus on NASA’s earth orbiting science programs.

Figure 1 summarizes the product platform leveraging strategies that are suggested by Meyer and Lehnerd.¹¹ In Figure 1, a generic market grid includes three market segments and three performance tiers. If commonalities are not considered in a product family design effort, an organization would have to independently develop nine different products to fully populate the market (Niche Platform Strategy). A Horizontal Leveraging Strategy allows components and subsystems from products serving the same performance tier to be shared across the different market segments. The main benefit of this strategy is that manufacturers could reduce cost due to sharing of R&D, development and manufacturing costs. A Vertical Leveraging Strategy allows capabilities to be scaled up and down and functionalities to be added or removed across performance tiers and within a single market segment. Knowledge gain from lower performance tiers can be used for the development of upper tiers components instead of starting afresh. Finally, a Beachhead Approach combines ideas from both horizontal and vertical leveraging strategies with the objective of market dominance.

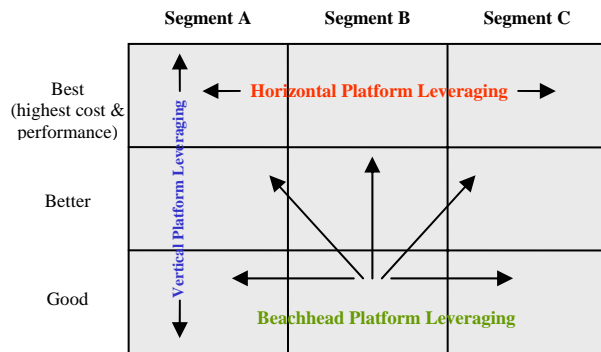


Figure 1: Leveraging strategies applied to the product platform segmentation grid (adapted from Ref. 10)

The objectives involved in the development of a commercial communication satellite product line, which is the focus of study in this paper, match the description of the Horizontal Platform Leveraging Strategy that is depicted in Figure 1. Here, a number of satellites with varying payload capacities must be designed in a coordinated way to maximize common components and subsystems while also maximizing the

performance of individual satellites to allow them to compete within their respective market segments. This problem could be formulated as a multiobjective design optimization problem and could benefit from recent developments in design optimization approaches implemented in the design of complex systems.

This paper presents a satellite product line architecting tool in which a multiobjective GA-based optimization approach is coupled with satellite performance estimation models to trade system level design variables of all product line members simultaneously. Specifically, the product line investigated in this work includes three communication satellites with three levels of payload requirements operating in C and Ku frequency bands, which are common for telephony and television services respectively. The three satellites considered in this work are referred to throughout this paper as the “small”, “medium”, and “large” satellites based on their minimum payload requirements, which are summarized in Table 1 below.

Table 1: Summary of payload requirements for the three satellites in a product line.

	small	medium	large
C-band HPAs	30	44	66
Ku-band HPAs	6	12	16
Antenna mass (kg)	100	140	180
Maximum antenna diameter (m)	2.8	3.2	3.6

There are 27 discrete design variables that describe each of the three satellites in the product line. Those 27 design variables can be grouped into three categories: 13 variables describe technology choices for payload and bus subsystems, one variable describes the choice of the launch vehicles, and 13 variables describe the redundancy levels implemented in the payload and bus subsystems. The design variables that describe each of the three satellites are summarized in Table 2. The design variables are self explanatory but some clarification is needed as to how the payload repeaters’ technology choices and redundancy levels are described as design variables.

In the three satellite sizes described in Table 1, the C-band repeaters are required to have large numbers of operating HPAs; therefore, a single switch matrix is not sufficient to operate redundant HPAs when any of the active HPAs fails. Consequently, the active C-band

HPAs are grouped into eight repeaters, each has its own switch matrix and redundant HPAs. Each of the C-band repeaters can use either a Traveling Wave Tube Amplifier (TWTA) or a Solid State Power Amplifier (SSPA) as the technology choice for its HPAs as described in design variables 1 to 8 in Table 2.

Table 2: Design variables for each of the three satellites in the product family.^{1, 2, 3}

Design Variable	Description and discrete values
1 to 8	HPA ^a type (TWTA ^b or SSPA ^c)
9	Launch vehicle (Ariane 5, Ariane 4, Sea Launch, Proton, Delta, Atlas, Long March, or H2A)
10	Solar array cell type (GaAs single junction, GaAs multi-junction, Si thin, Si normal, or hybrid Si with GaAs multi-junction)
11	Battery cell type (NiCd or NiH ₂)
12	N/S ^d Thermal Coupling (no coupling or coupling)
13	N/S STK ^e thrust technology (Xenon plasma, arcjets, bi-propellant, or hydrazine)
14	E/W ^f STK thrust technology (bi-propellant or hydrazine)
15	Redundancy level for Ku-Band transponder
16-23	Redundancy levels for each of the 8 C-Band transponders
24	Propulsion subsystem redundancy level (0 or full redundancy)
25	Attitude Determination & Control subsystem redundancy level (0 or full redundancy)
26	Telemetry, Command & Ranging subsystem redundancy level (0 or full redundancy)
27	Solar array area redundancy level (0%, 2%, 4% or 6% of solar array area)

^aHigh Power Amplifier, ^bTraveling Wave Tube Amplifier, ^cSolid State Power Amplifier, ^dNorth/South, ^eStation Keeping, ^fEast/West

Design variables 16 to 23 describe the redundancy levels for each of the eight C-band repeaters in each of the three satellites. These redundancy levels can be inferred by using both Table 2 and Table 3. For example, the medium size satellite has 44 required active C-band HPAs as shown in Table 2 and could have a maximum total of 66 available HPAs as shown in Table 3. This means that the number of redundant HPAs in the medium size satellite C-band repeater can vary from a minimum of zero units to a maximum of 22 units.

Table 3: Maximum available (active +maximum redundant) HPAs for payload repeaters for each of the three satellites in a product line.

	small	medium	large
Maximum available C-band HPAs	52	66	82
Maximum available Ku-band HPAs	10	16	20

In each of the three satellites, there is only one Ku-band repeater that includes all Ku-Band HPAs because the required operating number of HPAs is rather small and can be handled with a single switch matrix. The Ku-band HPAs can only use TWTAs for their technology choices.

The next two major sections of this paper describe the two building blocks of the satellite product line architecting tool, which are the optimization approaches implemented in this research and the satellite performance estimation models.

OPTIMIZATION TOOLS

GENETIC ALGORITHM (GA)

The GA is a global search method that mimics the behavior observed in biological populations.¹² The GA is modeled after Darwin's Theory of *Natural Selection*; it employs the principal of survival of the fittest in its search process, and it has been applied successfully to the design of many complex systems. The GA differs from conventional optimization methods in four different ways (adapted from Ref. 12) that make the GA well suited to the conceptual design of spacecraft product lines. First, the GA works with a coding for the design variables that allows for a combination of discrete and continuous parameters in one problem statement. Second, the GA needs only fitness or objective function values; no derivatives are needed. This feature not only allows for discrete variables, but also allows for discontinuous objective and constraint functions. Additionally, this property means that the GA provides no information about optimality of the solution. Third, the GA employs probabilistic choices rather than deterministic rules to find new points with likely improvement. This probabilistic search technique means that the GA is likely to search across the entire design space; it will not easily become trapped in local minima. Fourth, the GA is a population-based search technique, which results in multiple designs with good performance after each run of the GA, rather than only

one solution. Additionally, the population-based search nature of the GA means that several good solutions could be generated to characterize the tradeoffs encountered in multiobjective optimization problems.

MULTIOBJECTIVE OPTIMIZATION

In spacecraft design, or the design of any other complex system, there are usually several design objectives reflecting the interests of the various stakeholders. Those objectives evaluate the performance of various design concepts; in this research, the objectives evaluate various product families generated in the optimization run. If there is only one design objective, the design concept that measures the best against this objective should clearly be the concept of choice. However, when there are several competing design objectives, there are usually several good design concepts that measure differently against the individual objectives, but equally well against one measure that includes all the objectives. From the standpoint of a system engineer, it is highly desirable to obtain this set of design concepts, because they represent the tradeoffs between the various design objectives. An optimal tradeoff curve, surface or hypersurface depending on the number of objectives considered is commonly referred to as the Pareto front.¹³ For each of the Pareto-optimal set of designs, there is no other feasible design that is better on all objectives; in other words, these designs are non-dominated or non-inferior. For example, a high performance satellite design featuring little commonality within the product family can be at one end of the Pareto front while a design sharing a large amount of commonalities and has low performance can be located at the other end of the front. The goal in multiobjective design optimization problems is to minimize a vector function whose components are individual objectives as suggested by Equation 1.

$$\text{minimize } \phi(\mathbf{x}) = \begin{Bmatrix} \phi_1(\mathbf{x}) \\ \phi_2(\mathbf{x}) \\ \vdots \\ \phi_{N_{obj}}(\mathbf{x}) \end{Bmatrix} \quad (1)$$

Mathematically, in a minimization formulation for the objectives, a design with a vector of objectives \mathbf{V} dominates a design with a vector of objectives \mathbf{u} by meeting the conditions in Equation 2.

$$\text{if } \forall_i v_i \leq u_i \text{ and } \exists_i v_i < u_i \quad i = 1, 2, \dots, N_{obj} \quad (2)$$

The Pareto set of solutions are often plotted in objective space as shown in Figure 2. Here, ϕ_1 and ϕ_2

are objectives to be minimized. The area marked “feasible design space” represents the set of all feasible designs. The red curve, with the non-dominated Pareto optimal points, \mathcal{V} , represents the Pareto front which marks the boundary between the feasible design space and the infeasible design space. The two end points on the Pareto front are commonly referred to as anchor points and the direction that minimizes both objectives contains the utopia point. In Figure 2, point \mathcal{V} dominates point u because although the two points have the same value for ϕ_2 , point \mathcal{V} has a smaller value for ϕ_1 than point u .

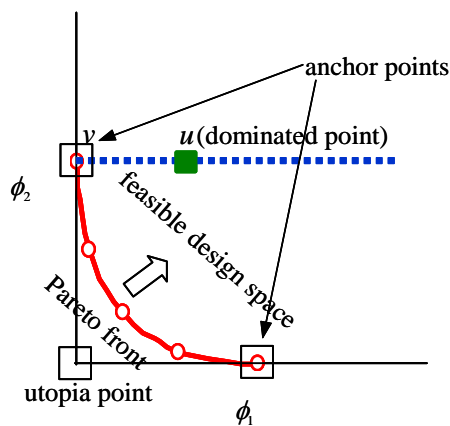


Figure 2: Graph depicting Pareto optimality.

There are several approaches to finding the Pareto optimal set using GAs. This research implements an approach called the “ N -Branch Tournament Selection GA”¹⁴, which exploits the population-based search of the GA to generate a large number of solutions to multiobjective problems in a single program run with nearly the same computational effort required to solve a single objective problem.² This tool was implemented in this research to simultaneously optimize four objective functions. The first objective is to maximize the common technology choices shared by all three satellites in the product line. The remaining three objectives minimize the launch mass values of the three individual satellites in the product line. Here satellite launch mass is taken as the performance metric for each satellite; other metrics could be used if they could be evaluated using satellite performance estimation models.

GA FOR ARCHITECTING PRODUCT FAMILIES

There have been other research efforts that investigated the design of product families using a GA-based approach. One recent contribution in this field is that of Simpson and D’Souza^{6,15} who investigated the design of a family of general aviation aircraft with variable seating capacity. This work has demonstrated the successful use of multiobjective GA for the design of product families. However, Simpson and D’Souza’s approach restricted the common design parameters between the product family to a subset that was chosen prior to the optimization run using a design of experiments approach. Commonality was controlled by a dedicated commonality substring within the chromosome. The values of this set of common variables were then optimized for the product family using the GA. This approach can only produce sub-optimal solutions rather than global ones because design parameters were optimized for only one aircraft configuration. To avert this shortcoming, the whole set of possible configurations with their associated design parameters for the members of the product family must be traded off in an optimization process to decide on the global optimum solution. In the research presented here, all combinations of satellite configurations are considered in the optimization run. This approach will allow for a near-global optimum solution for the product family design problem. The term near-global is used because there is no proof of optimality with the GA as it is a non-gradient-based method.

In this work, each chromosome describes three spacecraft comprising a product line that serves three different market segments. In other words, each chromosome is divided into three sub-chromosomes of equal length. Each sub-chromosome describes the technology choices and redundancy levels of one of the spacecraft. Each sub-chromosome describes a total of 27 design variables that are encoded into 41 binary bit strings. Of the 27 design variables that describe each of the spacecraft in a product line, 13 variables describe the technology choices for components and subsystems, one describes the choice of the launch vehicle, and 13 describe redundancy levels for components and subsystems. The commonality in each product line is evaluated based on the number of common technology choices shared by the three sub-chromosomes that describe three spacecraft sizes. There is a maximum of 13 technology choices that can be shared among all three sub-chromosomes or spacecraft sizes as depicted in Figure 3. This chromosome structure describes 81 design variables (27 variables for each satellite) and is encoded using 123 binary bit strings (41 bits for each

satellite). The encoding approach described in Figure 3 is implemented with the multiobjective optimization tool “N-Branch Tournament Selection GA”^{14,2} and the satellite performance estimation models are described in the following section to optimize the three unit satellite product line configurations.

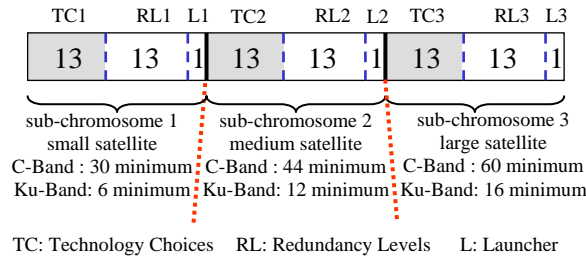


Figure 3: Representation of chromosome structure for a family of communication satellites.

SPACECRAFT PERFORMANCE ESTIMATION

Few computational tools are readily available to predict spacecraft system level performance metrics such as mass, power, size, and reliability. Existing tools, if publicly available, are only capable of sizing specific classes of spacecraft. To the authors’ best knowledge, a high fidelity tool that is capable of sizing all classes of geosynchronous communication satellites with wide range of payload types and capacities is not available publicly. Such computational tool is needed to evaluate the performance of spacecraft architectures generated during the product family optimization run. In this preliminary work, the authors opted to use a satellite sizing tool that was developed by the first author of this paper in her doctoral work¹ to specifically size medium size commercial communication satellites. In this product family design research, the tool was used to size spacecraft with small or large payload in addition to its original task of sizing medium size spacecraft. Future work will include the development of a higher fidelity tool that is based on a wide range of historical data describing all spacecraft sizes.

The next two subsections describe in detail the original tool that was developed by the first author to size medium size spacecraft and is largely based on the author’s industrial experience and the basic approach outlined in Space Mission Analysis and Design by Wertz and Larson¹⁶. The satellite design tool consists of a satellite sizing model that predicts spacecraft mass, power, and size, and a satellite reliability prediction model. This satellite design tool is coded into MATLABTM scripts and is coupled with the GA tools

that were described in the previous section of this paper and are also coded in MATLABTM scripts. In many of the following design estimating relationships, scaling factors are used to correlate a basic prediction (e.g. repeater weight) to actual values from a database of existing geosynchronous communication satellites. The data for these known satellites is proprietary and cannot be shared here.

SATELLITE SIZING MODEL

The sizing tool predicts system level parameters for geosynchronous communication satellites, i.e. launch mass, required power, and size. The three satellite design missions (product family) that are under investigation in this research provide telecommunication services in C and Ku frequency bands common for telephony and television. In the absence of cost models for commercial communication satellites, the estimated launch mass of the satellites product family members will be used as design objectives. In 1998, the estimated cost of launching one kg of payload into its orbital position ranged from \$22,500 to \$30,000.¹⁷ Furthermore, launch insurance is typically 25% of launch cost. The high launch cost means that launch mass could be considered as a surrogate for cost. Alternatively, satellite designers would often work with a fixed launch mass based on the choice of a launch vehicle and try to maximize payload mass.

Payload Sizing

Antennas and repeaters comprise the payload of a communication satellite. In the sizing model, antenna sizing is treated as a designer input because antenna design is mission specific. Determining specific antenna sizes requires running a commercial code that was not available during the course of this work. Payload antennas are shaped to provide different Effective Isotropic Radiated Power (EIRP) rates for a number of coverage areas based on market requirements, mission objectives and telecom applications. For higher satellite transmitted EIRP, the receiving antenna on Earth is smaller. While higher EIRP rates are favorable, they require large amount of repeater input DC power, which is limited by solar arrays and batteries capabilities.

In this study, the results of antenna design tools are fed to the satellite sizing tool in terms of different coverage areas’ antenna gain values. Also for each of the coverage areas, the required EIRP rate is supplied to the sizing tool along with a standard estimate of the Transmitter-to-Antenna line power Loss (LTA). Using

this information, the sizing tool calculates the output Radio Frequency (RF) power, P_{RF} , that must be supplied by each active HPA designated to a given coverage area as described in Equation 3.

$$P_{RF} \text{ (in dBW)} = EIRP - Gain + LTA \quad (3)$$

Two types of HPAs are modeled in the sizing tool, TWTA and SSPA. Based on the type of the HPA with standard efficiencies, η_{HPA} , and the calculated values of required HPA output RF power (from Equation 3), the input power required to operate the HPA can be calculated. An average TWTA efficiency is about 57% in Ku-band and 52% in C-band, whereas an average SSPA efficiency is about 35% in C-band. To date, TWTAs are the only option for Ku-band HPAs; the sizing code follows this idea. To calculate the required overall repeater input DC power for each coverage area, the electric power conditioning (EPC) efficiency, η_{EPC} , has to be accounted for (about 93% on average). The HPA input DC power, P_{DC} , is then calculated as shown in Equation 4.

$$P_{DC} \text{ (in dBW)} = \frac{P_{RF}}{\eta_{HPA} \eta_{EPC}} \quad (4)$$

If an HPA is intended to operate at some Output-Back-Off (OBO) power, say 3 dB, the input DC power is generally reduced compared to the required power for an HPA working at normal mode (saturation). If the HPA is a TWTA, the 3 dB OBO required input power scaling factor, f_{OBO} , is equal to 75%; whereas, if it is an SSPA, the 3 dB OBO input power scaling factor is equal to 95%. Therefore, the number of HPAs working at 3 dB OBO, HPA_{OBO} , out of the total number of active HPAs, HPA_{active} , for each coverage area (repeater) must be specified. In the presence of HPAs working at 3 dB OBO, the total input DC power for a repeater, $P_{repeater}$, of a given coverage area with a total of HPA_{active} channels, can be calculated as shown in Equation 5.

$$P_{repeater} = P_{DC} (HPA_{OBO} f_{OBO} + (HPA_{active} - HPA_{OBO})) \quad (5)$$

The power lost from the HPAs and the EPCs is transformed into heat that is dissipated by the thermal radiators of the bus. The heat flow rate, $\dot{Q}_{repeater}$, can be calculated as shown in Equation 6.

$$\dot{Q}_{repeater} \text{ (in dBW)} = P_{RF} HPA_{active} - P_{repeater} \quad (6)$$

Although TWTAs have higher efficiencies (which means less heat dissipation and lower required input

DC power) than SSPAs for the same output RF power, TWTAs are about twice as heavy as SSPAs. The type of the HPA and the total number of HPAs for each coverage area (including the number of active HPAs, HPA_{active} , and the number of redundant ones, $HPA_{redundant}$) is used to calculate the overall repeater mass, $M_{repeater}$, as shown in Equation 7.

$$M_{repeater} \text{ (in kg)} = SF_1 M_{HPA} (HPA_{active} + HPA_{redundant}) \quad (7)$$

Where M_{HPA} is the mass of one HPA. Here the number of redundant HPAs is a design variable. The repeater mass, $M_{repeater}$, includes the mass of all available HPAs and all other repeater components such as channel amplifiers, frequency converters, multiplexers, switches, fasteners, and brackets. In Equation 7, a scaling factor, SF_1 , accounts for all other components in the calculation of the overall repeater mass for each coverage area.

Finally, the overall payload required input DC power, dissipated heat, and mass, can be calculated as shown in Equations 8, 9, and 10 respectively. These equations use the calculations for each repeater (there is one repeater for each coverage area and each repeater has several HPAs), which are shown in Equations 5 through 7. The output of payload sizing in terms of payload required input DC power, dissipated heat, and mass is used for sizing bus subsystems.

$$P_{payload} \text{ (in dB)} = \sum_{i=1}^{N_{repeaters}} P_{repeater_i} \quad (8)$$

$$\dot{Q}_{payload} \text{ (in dBW)} = \sum_{i=1}^{N_{repeaters}} \dot{Q}_{repeater_i} \quad (9)$$

$$M_{payload} \text{ (in kg)} = M_{antennas} + SF_2 \sum_{i=1}^{N_{repeaters}} M_{repeater_i} \quad (10)$$

In Equation 10, the mass of the antennas, $M_{antennas}$, is mission specific and therefore is an input to the sizing tool as was specified in Table 1. A scaling factor, SF_2 , is used in Equation 10 to account for the repeaters integration mass.

Although the scaling factors used in the calculations of the payload mass and in the remaining calculations implemented in the satellite sizing tool in general are empirical and are based on a small number of existing missions, the sizing framework is appropriate for the conceptual design stage and can use any other values for the scaling factors. Better scaling factors can be readily implemented if more information

is available from a larger number of missions and a wider range of spacecraft sizes.

Bus Sizing

Bus sizing is the second part of the sizing tool. The spacecraft bus includes six major subsystems: the Electrical Power Subsystem (EPS), the thermal subsystem, the propulsion subsystem, the Attitude Determination and Control Subsystem (ADCS), the Telemetry, Command and Ranging (TCR) subsystem, and the structures and mechanisms subsystem.

To size the bus geometrically, the satellite sizing tool uses two pieces of information: the size of the launch vehicle fairing envelop and the size of the largest satellite side wall antenna (usually positioned on the East/West (E/W) panels of the satellite). Figure 4 illustrates the panel naming convention. The maximum sidewall antenna diameter is mission specific and is an input to the sizing tool as was described in Table 1. The available payload (here refers to the launch vehicle payload, i.e. the satellite) envelope controls the size of the solar arrays, because they are usually attached to and stowed against the North/South (N/S) panels as shown in Figure 5. The envelope also affects the size of the thermal radiator, because the N/S panels are used as radiation surfaces to expel heat generated within the satellite.

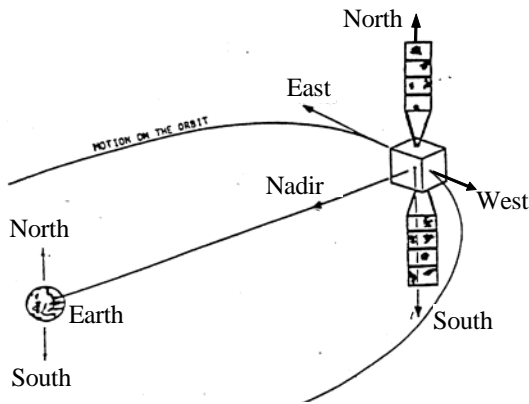


Figure 4: Satellite position in orbit showing panel naming convention.

Equation 11 describes the relation between the sidewall antenna diameter, the launch vehicle fairing diameter and the N/S panel width, $W_{N/S}$.

$$W_{N/S} (in m) = 2\sqrt{r^2 - y^2} \quad (11)$$

where r (in m) = fairing radius

$$y (in m) = \frac{side\ wall\ antenna\ diameter + 0.2}{2}$$

Equation 11 is derived by analyzing a top view of the stowed configuration of the satellite inside the launch vehicle fairing. The value of 0.2 m that is added to the side wall antenna diameter in Equation 11 accounts for a 20 cm allowance for the solar array stowage from both sides. The height of the fairing determines the maximum length of the solar array panels and the maximum height of the thermal radiators as illustrated in Figure 5.

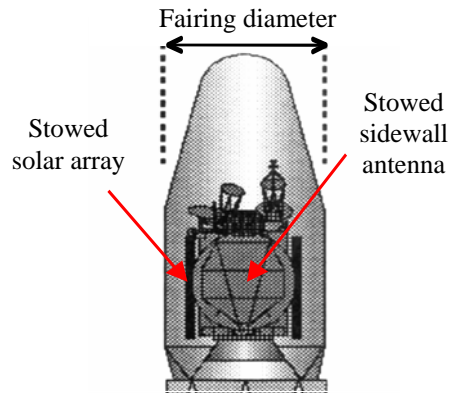


Figure 5: Stowed satellite configuration in launch vehicle fairing (adapted from Ref.18).

There are eight choices for the launch vehicle implemented in the sizing tool: Ariane 5, Ariane 4, Sea Launch, Proton, Delta, Atlas, Long March, and H2A. The information of each launch vehicle including fairing geometry, maximum lift mass and ΔV , are specified in the sizing tool. ΔV represents the change of velocity the satellite needs to achieve to move itself in the transfer orbit after separation from the launch vehicle to its final location in the geosynchronous orbit.

After defining the geometry of the bus, the sizing model estimates satellite power, P_{sat} , dissipated heat flow rate, \dot{Q}_{sat} , and dry mass, M_{dry} , based on payload power, heat flow rate and mass as shown in Equations 12 through 14 respectively.

$$P_{sat} (in W) = SF_3 10^{P_{payload} / 10} \quad (12)$$

$$\dot{Q}_{sat} (in W) = SF_4 10^{\dot{Q}_{payload} / 10} \quad (13)$$

$$M_{dry} (in kg) = SF_5 M_{payload} \quad (14)$$

Here SF_3 , SF_4 , and SF_5 are empirical scaling factors. The total power during normal operations (sunlight) is

estimated using a larger value for SF_3 than the value used to estimate the total required satellite power during eclipse time. This is because the solar arrays are required to produce additional power to charge the batteries during sunlight.

The satellite dry mass is then used to estimate the mass of four subsystems of the satellite (ADCS, TCR, propulsion and structures) using scaling factors. These scaling factors have been selected so that the sizing tool reasonably estimates mass of existing geosynchronous communication satellites from a proprietary database. The total mass of these four bus subsystems add up to 35% of the satellite dry mass. The mass values of the remaining two subsystems, namely the EPS - including solar arrays and batteries - and thermal subsystem, are estimated more accurately based on the total required satellite power and the dissipated heat from the payload and the bus subsystems.

Electrical Power Subsystem Sizing

The electrical power subsystem sizing includes solar array sizing and battery sizing. Solar array sizing requires four parameters: total required sunlight DC power (estimated from Equation 12), solar cell type, number of panels in each array, and required Operational Maneuver Life (OML) in years. There are two available solar array cell types: Silicon (Si) and Gallium Arsenide (GaAs). The choice of the cell type specifies the Beginning of Life (BOL) cell power, $P_{cell_{BOL}}$ and the performance degradation factor, DF , due to radiation.

The solar cell End of Life (EOL) power output, $P_{cell_{EOL}}$, can be calculated as shown in Equation 15. The area of the solar array, A_{SA} , can then be calculated by dividing the total required sunlight power by the EOL cell power (worst case scenario) as shown in Equation 16.

$$P_{cell_{EOL}} \text{ (in } W/m^2 \text{)} = (1 - DF)^{OML} P_{cell_{BOL}} \quad (15)$$

$$A_{SA} \text{ (in } m^2 \text{)} = \frac{P_{sat}}{P_{cell_{EOL}}} \quad (16)$$

The total solar array mass includes the mass of the solar cells, substrate, deploying mechanisms, and connections. The mass of the solar cells, M_{cell} , can be estimated by multiplying the mass of one square meter of cells by the solar array area, A_{SA} . To account for the mass of the substrate, deploying mechanisms, and connections in the calculation of the overall solar array

mass, M_{SA} , the mass of the cells is scaled up by a factor SF_6 as shown in Equation 17. Typically, there are four or five panels per array. The deployed length of the array, L_{SA} , and hence the length of each panel, can then be calculated by dividing the calculated area of the array by the width of the N/S panels, $W_{N/S}$, as shown in Equation 18.

$$M_{SA} \text{ (in kg)} = SF_6 M_{cell} A_{SA} \quad (17)$$

$$L_{SA} \text{ (in m)} = \frac{A_{SA}}{W_{N/S}} \quad (18)$$

Although GaAs has higher output power per square meter, it weighs about twice as much as Si cells, and GaAs is also more expensive. A recent trend in the design of geosynchronous communication satellites is to use hybrid solar arrays that have few panels made of GaAs and the rest made of Si. Assuming all the panels have equal areas, a number of Si panels N_{Si} , and a number of GaAs panels N_{GaAs} , Equations 16 and 17 can be re-written as shown in Equations 19 and 20 respectively.

$$A_{SA} = \frac{P_{sat}}{(N_{Si} + N_{GaAs})} \left(\frac{N_{Si}}{P_{Si_{EOL}}} + \frac{N_{GaAs}}{P_{GaAs_{EOL}}} \right) \quad (19)$$

$$M_{SA} \text{ (in kg)} = \frac{SF_6 A_{SA}}{(N_{Si} + N_{GaAs})} (N_{Si} M_{Si} + N_{GaAs} M_{GaAs}) \quad (20)$$

The second part of EPS sizing is battery sizing. Batteries are used onboard of the satellite to provide power to satellite equipment during eclipse time. Solar arrays charge the batteries during sunlight. Battery sizing begins by choosing the type of battery cell. Traditional battery cell types in geosynchronous communication satellites are Nickel Cadmium (NiCd) and Nickel Hydrogen (NiH₂). The lower the Depth of Discharge (DOD) value is, the more capacity the battery cell can handle. NiCd battery cells have higher DOD than NiH₂ cells. Geosynchronous communication satellites always have two separate units of battery cells; both work simultaneously in eclipse time, but if one fails, the other can only support the subsystems that would keep the satellite in its orbital position until the end of eclipse (maximum eclipse time, $T_{eclipse}$, for the geosynchronous orbit is 72 minutes).

The number of battery cells, $N_{battery\ cells}$, in each unit usually varies between 25 to 35 cells depending on the DOD and the required satellite power during eclipse time (calculated in Equation 12). For reliability considerations, a redundant cell is added to each of the

battery units. Using a given discharge voltage per cell, V_d , a diode loss, L_d , battery capacity in Amp-hour, $C_{battery}$, can be calculated as shown in Equation 21.

$$C_{battery} = \frac{P_{sat} T_{eclipse}}{2 DOD (V_d (N_{battery\ cells} - 1) - L_d)} \quad (21)$$

The mass of the batteries, $M_{battery}$, can be calculated based on the capacity in W-hour as shown in Equation 22 where SF_7 is determined by the cell type.

$$M_{battery} (in\ kg) = \frac{2 C_{battery} V_d N_{battery\ cell}}{SF_7} \quad (22)$$

Finally, the total mass of the electrical power subsystem, M_{EPS} , is the sum of the solar array mass and the battery mass in addition to the mass of the power conditioning units, processors, and the electrical as well as the mechanical integration. These are accounted for by the scaling factor, SF_8 , as shown in Equation 23.

$$M_{EPS} (in\ kg) = SF_8 (M_{SA} + M_{battery}) \quad (23)$$

Thermal Subsystem Sizing

The thermal subsystem radiates the heat produced by both the payload and the bus to ensure that all the satellite components remain at their nominal operational temperatures. The thermal radiators are placed on the N/S panels of the satellite. Since the North panel is more exposed to the sun than the South panel, sometimes N/S thermal coupling is implemented to transfer some heat from the North panel payload to the cooler South panel radiator. This adds the mass of the heat pipes to the thermal subsystem mass, but allows more heat transfer out of the spacecraft for a given radiator area or allows for a small radiator area for a given amount of heat flow rate.

The sizing tool uses Stefan-Boltzmann Law to estimate the area of the thermal radiators. This involves estimating the heat flow rate from the spacecraft, \dot{Q}_{sat} , as described in Equation 13. The material of the thermal radiators specifies the surface emissivity, e . The maximum hot temperature of the outer sink (vacuum), T_{HS} , is 236.84 K. The radiator maximum temperature, $T_{radiator}$, is approximated in the model as 328 K. When there is no thermal coupling, the area of each radiator, $A_{radiator}$, can be calculated as shown in Equation 24.

$$A_{radiator} (in\ m^2) = \frac{0.5 \dot{Q}_{sat}}{e s (T_{radiator}^4 - T_{HS}^4)} \quad (24)$$

In Equation 24, s is Stefan-Boltzmann constant, which is equal to $5.67 \times 10^{-8} W/m^2 K^4$. The calculation in Equation 24 assumes worst case scenario, i.e. the sizing is based on the temperature of the North radiator, T_{HS} , which is hotter than the South Radiator (because of sun exposure). This approach oversizes the area of the South radiator. When thermal coupling is employed, some amount of heat flow rate is transferred from the North panel payload to the South radiator. This decreases the amount of heat that must be radiated from the hot North panel, and therefore decreases the required radiator area for worst case design.

The radiator height, $H_{radiator}$, can be estimated based on the calculated radiator area, $A_{radiator}$, from Equation 24 and based on the calculated N/S Panel width, $W_{N/S}$, from Equation 11 as shown in Equation 25. The radiator height must not exceed the height of the launch vehicle fairing. Finally, the mass of the thermal subsystem is estimated based on the radiator area, radiator depth, $d_{radiator}$, and an estimate of the radiator material density, $\rho_{radiator}$, as shown in Equation 26. When N/S thermal coupling is employed, the mass of the thermal subsystem increases as it includes the mass of the heat pipes running from the North panel to the South panel.

$$H_{radiator} (in\ m) = \frac{A_{radiator}}{W_{N/S}} \quad (25)$$

$$M_{thermal} (in\ kg) = \rho_{radiator} d_{radiator} A_{radiator} \quad (26)$$

At this point, a refined estimate of the bus can be made as shown in Equation 27. The bus mass includes the calculated masses of the structure subsystem, the propulsion subsystem, the attitude determination and control subsystem (ADCS), the electrical power subsystem (EPS), the thermal subsystem, the Telemetry, Command and Ranging (TCR) subsystem. The satellite dry mass includes the mass of the payload and the mass of the bus. It is a standard practice to add a 5% margin to the estimated dry mass during conceptual design as shown in Equation 28. The sizing tool follows this practice.

$$M_{bus} (in\ kg) = M_{structure} + M_{propulsion} + M_{ADCS} + M_{EPS} + M_{thermal} + M_{TCR} \quad (27)$$

$$M_{dry} (in\ kg) = 1.05 (M_{payload} + M_{bus}) \quad (28)$$

Propellant Sizing

Propellant sizing determines the mass of the propellant needed for the spacecraft during its entire mission. There are two main propellant sizing steps. The first one determines the propellant needed during the transfer orbit; this quantity is mainly dependent on the transfer orbit provided by the launch vehicle. The standard technology to enter the geosynchronous orbit from the transfer orbit is a Liquid Apogee Engine (LAE), which utilizes bi-propellant thrusting. The satellite sizing tool assumes that this is the only option for orbit insertion. Based on the choice of the launch vehicle, the change in velocity, ΔV , needed for the transfer orbit is determined and is usually achieved in two or three apogee firings. The ΔV needed to reach the geosynchronous orbit from the transfer orbit ranges from 1464 to 1828 m/s based on the choice of the launch vehicle.

The second main propellant sizing activity determines the amount of propellant needed for Station Keeping (STK) and attitude control of the satellite during its OML. STK for a geosynchronous communication satellite commonly confines the satellite within a 1° wide square around its desired orbital location at all times. STK is usually performed every two weeks or once a month, based on the operational plan. Staying within the 1° square involves N/S STK and E/W STK. The N/S STK ΔV is the more demanding maneuver requiring about 45 m/s/year, while the E/W STK ΔV maneuver requires about 1.5 m/s/year. The attitude control consumes very little propellant each year; it is less than one kg/year. These values are based on historical geosynchronous satellite requirements and are implemented in the sizing tool.

The rocket equation provides the estimate for propellant mass, $M_{propellant}$. An initial estimate of the satellite wet mass, $M_{initial}$, is needed to begin an iterative process as shown in Equations 29 and 30. A quick survey of recent missions revealed that if the N/S STK uses plasma propulsion, the wet mass is about twice as much as the total dry mass, whereas for every other type of propulsion technology (arcjets, bi-propellant thrusters, or hydrazine thrusters), the wet mass is about two and half times the dry mass. This estimated wet mass is used in the rocket equation along with the specific impulse, I_{sp} , and the efficiency of the thrusters, $\eta_{thruster}$, to estimate the mass of propellant used in the three firings of the LAE during the transfer orbit. The LAE propulsion assumes a liquid bi-propellant.

$$M_{final} / M_{initial} = e^{-\Delta V / (g I_{sp} \eta_{thruster})} \quad (29)$$

$$M_{propellant} \text{ (in kg)} = M_{initial} - M_{final} \quad (30)$$

The propellant needed for STK and attitude control operations is calculated based on required ΔV on a yearly basis. The rocket equation is used for these calculations; the I_{sp} and the efficiency of the system vary with the type of the propulsion technology. For N/S STK, there are four propulsion choices: plasma (Xenon), arcjets, bi-propellant, and hydrazine thrusters. Plasma has the highest I_{sp} and lowest efficiency whereas Hydrazine thrusters have the lowest I_{sp} and a standard efficiency. For the E/W STK, bi-propellant thrusters and hydrazine thrusters are available. Finally, the wet (launch) mass of the satellite can be estimated as shown in Equation 31. The satellite total launch mass is used as an objective function in the optimization problem formulation. $M_{adaptor}$ is the mass of the adaptor that mounts the satellite to the launch vehicle; it is taken here as 50 kg.

$$M_{wet} \text{ (in kg)} = M_{dry} + M_{propellant} + M_{adaptor} \quad (31)$$

SATELLITE RELIABILITY MODEL

While approaches to predict satellite reliability exist, none appear to be available in open publications or as a computer code. In order to compute satellite reliability values for each of the three communication satellites in the product line, standard approaches were taken and coded into MATLAB™ scripts. This reliability model is also taken from the first author's doctoral dissertation. The reliability model calculates the reliability of each subsystem based on the type of technology it utilizes and the level of redundancy implemented in the design of that subsystem. The reliability model first calculates payload reliability, bus subsystems reliabilities, and then overall system reliability. Launch vehicle reliability is also incorporated as a design constraint. Some of the reliability values used in this model are assumed because failure rates for some components and subsystems are not available in published data. The assumptions are made based on the first author's experience in the satellite industry. For alternative technologies that are available for the same component or subsystem, higher reliability values are assigned to the older, more commonly used technologies and lower reliability values are assigned for the relatively new technologies, if no additional information was available. It is assumed that in an actual spacecraft

design setting, these assumed failure rates would be replaced by better information available to the spacecraft manufacturer.

A study by Goddard Space Flight Center showed an average of 1.7 failures per spacecraft during the first 30 days compared to an average of less than 0.2 failures per spacecraft per month during the following five months.¹⁹ The high failure probability in the early stage of operation is due to the fact that design problems are more likely to become apparent in the early phase of operation. The failure of any component or subsystem in the spacecraft during launch or orbit insertion has a much larger effect on the rest of the mission than failures in later phases of the mission. Therefore, this research uses reliability values at the end of the 30th day of on-orbit operation to compute payload and system reliability values.

Payload reliability is computed from the reliability of the antennas and repeaters serving all coverage areas. Each repeater's reliability is calculated based on the type of the HPA and the number of the active HPAs out of the number available aboard the satellite. The reliability of one HPA at the end of the first month of operation is calculated using an exponential distribution as shown in Equation 32. The failure rate, λ , is 660 or 880 failures per billion amplifier operating hours for TWTA or SSPA, respectively.²⁰ This indicates that the reliability of a TWTA is higher than that of an SSPA. At $t = 30$ days, the reliability values for TWTAs and SSPAs that are implemented in the reliability model are 99.95% and 99.94% respectively.

$$R(t) = e^{-\lambda t} \quad (32)$$

Equation 33 is used to calculate total repeater reliability, $R_{repeater}$, from individual HPA reliabilities, R_{HPA} , for M active HPAs out of N available ones. This M -out-of- N approach is often employed for spacecraft payloads. For example if 12 HPAs were needed for a repeater and 16 HPAs were available, $M = 12$ and $N = 16$ would be used in Equation 33 to compute repeater reliability.

$$R_{repeater} = \sum_{i=M}^N \binom{N}{i} R_{HPA}^i (1 - R_{HPA})^{N-i} \quad (33)$$

To calculate the overall payload reliability, all repeaters and antenna reliabilities are multiplied as shown in Equation 34. Because antenna design is not part of the satellite sizing tool, the reliability values of antennas are taken to be equal to 100%.

$$R_{payload} = R_{antennas} \times R_{repeaters} \quad (34)$$

The bus reliability is a function of its six subsystems reliabilities. The reliability of the structures subsystem, $R_{structure}$, is assumed to be 99.00%. This value was also assumed for both the Attitude Determination and Control Subsystem (ADCS) reliability, R_{ADCS} , and the Telemetry, Command, and Ranging (TCR) subsystem reliability, R_{TCR} . In the reliability model, both ADCS and TCR can either be stand-alone systems or they can both have full duplicate redundancies, the reliability of which can be calculated from the single system reliability, R_s , as in Equation 35.

$$R_{(1-out-of-2)} = 2R_s - R_s^2 \quad (35)$$

The reliability of Electrical Propulsion Subsystem (EPS) is the product of the solar array reliability and the battery reliability. For the solar array, it is assumed that Si cells have higher reliability than GaAs because GaAs cells are relatively new in the industry compared to Si cells. The area of additional cell strings used to replace any failed string represents redundancy for the solar arrays. In the satellite industry, a 5% additional solar array area is typically used for redundancy. The satellite reliability model allows for four options: no redundancy, 2% redundancy in solar array area, 4%, or 6%. The solar array reliability value is computed based on the M -out-of- N approach as shown in Equation 36. Here $M = 100\%$ representing total required solar array area, and $N = 100\%$, 102%, 104%, or 106% representing redundancy options.

$$R_{solar\ array} = \sum_{i=M}^N \binom{N}{i} R_{cell}^i (1 - R_{cell})^{N-i} \quad (36)$$

For Hybrid solar arrays, the cell reliability value used in Equation 36 is implemented in the sizing tool as a weighted average of Si cell reliability (99.00%) and GaAs cell reliability (98.50%) as shown in Equation 37. Here N_{Si} is the number of Si solar array panels and N_{GaAs} is the number of GaAs panels.

$$R_{cell} = \frac{N_{Si} R_{Si}}{(N_{Si} + N_{GaAs})} + \frac{N_{GaAs} R_{GaAs}}{(N_{Si} + N_{GaAs})} \quad (37)$$

As for battery reliability, NiH₂ cells are assumed to have higher reliability (99.00%) than NiCd cells reliability (98.00%) because NiH₂ cells have a longer use history in commercial space applications. The EPS reliability value can be calculated as shown in Equation 38.

$$R_{EPS} = R_{solarArray} R_{battery} \quad (38)$$

The reliability of the thermal subsystem, $R_{thermal}$, is a function of its complexity. If the thermal subsystem employs N/S thermal coupling, then its reliability value (97.37%) is less than the reliability of the no-coupling option (99.30%) because this additional component provides another failure mode.²¹

As for the propulsion subsystem, it is assumed that bi-propellant thrusters have the highest reliability value (99.93%), followed by hydrazine thrusters (99.50%), arcjets (99.00%), and finally the new plasma thrusters (98.50%). The propulsion subsystem included in the reliability model is used for station keeping and attitude control. The propulsion subsystem can either have one branch of thrusters or two fully redundant branches. If two branches of thrusters are used, Equation 35 predicts the propulsion subsystem reliability, $R_{propulsion}$. Most commercial satellites are designed with two branches. Because the reliability model calculates the system reliability at the end of the 30th day after launch, the Liquid Apogee Engine (LAE) is not accounted for in reliability calculations as it is used to move the satellite from its transfer orbit to its orbital location in the geosynchronous orbit and that usually occurs before the end of the first month after launch.

The bus reliability, R_{bus} , and the spacecraft reliability, $R_{spacecraft}$, can be calculated as shown in Equations 39 and 40.

$$R_{bus} = R_{structure} R_{ADCS} R_{TCR} R_{EPS} R_{thermal} R_{propulsion} R_{harness} \quad (39)$$

$$R_{spacecraft} = R_{payload} R_{bus} \quad (40)$$

Usually, failure during launch is covered by insurance and the launch service provider may offer the satellite owner another free launch, but this does not reflect the actual losses due to failure. Investigations to establish responsibility for mission failure usually delay insurance reimbursement. During this time, the satellite operator may lose revenue and customers until a replacement satellite is built and deployed, which can take about two to three years on average.²² Choosing a highly reliable launch vehicle may be worth the high cost, when the risk associated with failure is considered. Therefore, the launch vehicle reliability is included in the reliability model assembled for this research and is treated as a design constraint.

Each of the available launch vehicles has a figure of merit representing its reliability based on the number of successful launches out of overall number of launches until 1999²³. Launch vehicles that have less than 50 successful launches were penalized an additional 25% below the 1999 published success rate.

This somewhat arbitrary strategy was used to discriminate against launchers that have a high success rate with low number of launches. Other strategies could be implemented, if enough data was available. The reliability rate for the eight launch vehicles, namely, Ariane 5, Ariane 4, Sea Launch, Proton, Delta, Atlas, Long March, and H2A, are 8%, 97%, 75%, 88%, 98%, 75%, 85%, and 58% respectively.

PROBLEM STATEMENT

The optimization tools and the satellite performance estimation tools described in the previous two major sections are coupled to optimize a geosynchronous communication satellite product line with three varying payload requirements that are described in Table 1. There 81 design variables describing technology choices, launch vehicle choices, and redundancy levels for all three satellites in the product line. These 81 design variables are encoded in 123 binary bit strings that can be combined in $2^{123} = 10^{37}$ product family architectures. Table 2 summarizes the 27 design variables describing each of the three satellites. There are four objective functions that are optimized simultaneously using the *N*-Branch Tournament Selection GA¹⁴; these objectives are described in Equations 41 to 44. The first objective maximizes the number of common technology choices among the three satellite sizes in the product line. However, a minimization formulation is used for the objectives; hence, a negative sign must be added to the first objective. The remaining three objectives minimize the launch mass of each satellite.

$$\phi_1(\mathbf{x}) = - \text{Number of Common Technology Choices} \quad (41)$$

$$\phi_2(\mathbf{x}) = \text{Small Satellite Launch Mass} \quad (42)$$

$$\phi_3(\mathbf{x}) = \text{Medium Satellite Launch Mass} \quad (43)$$

$$\phi_4(\mathbf{x}) = \text{Large Satellite Launch Mass} \quad (44)$$

There are 18 constraint functions; six for each of the three satellites. Those constraints are described in Equations 45 to 50. The first and second constraints ensure that the solar panel length and the radiator panel height computed by the satellite sizing model do not exceed the height of the fairing of the launcher as expressed mathematically in Equations 45 and 46, respectively and as demonstrated in Figure 5.

$$g_1(\mathbf{x}) = \frac{L_{SA}}{\text{Fairing Height}} - 1 \leq 0 \quad (45)$$

$$g_2(\mathbf{x}) = \frac{H_{radiator}}{\text{Fairing Height}} - 1 \leq 0 \quad (46)$$

The maximum allowable lift mass of the launch vehicle is used as a constraint on the satellite total wet mass, which is expressed in Equation 47. Two additional reliability measures are treated as constraints. The reliability of the launcher based on the number of successful launches out of the total number of launches was included, because this is generally a specific mission requirement. A minimum reliability of 90% was chosen to represent high launch vehicle reliability requirement; this is shown in Equation 48.

$$g_3(\mathbf{x}) = \frac{M_{wet}}{\text{Maximum Lift Mass}} - 1 \leq 0 \quad (47)$$

$$g_4(\mathbf{x}) = 1 - \frac{\text{Launcher Reliability}}{90\%} \leq 0 \quad (48)$$

Finally, two constraints are imposed on the satellite payload reliability and the overall satellite reliability to be greater than 99% and 90% respectively as shown in Equations 49 and 50. Even though payload reliability is part of spacecraft reliability, this payload reliability constraint is added because payload reliability, separate from total spacecraft reliability, is generally a requirement for marketing competitiveness to ensure availability.

$$g_5(\mathbf{x}) = 1 - \frac{R_{payload}}{99\%} \leq 0 \quad (49)$$

$$g_6(\mathbf{x}) = 1 - \frac{R_{spacecraft}}{90\%} \leq 0 \quad (50)$$

The constraints in Equations 45 through 50 are formulated such that they are negatively valued when they are satisfied. Each set of constraints (there are three sets) is handled using external linear penalty function formulation, which means that the N -Branch Tournament Selection GA handles four fitness functions (one unconstrained and three constrained) as shown in equations 51 through 54. The subscripts small, medium and large in Equations 52 to 54 refer to the product line three satellite sizes. This formulation penalizes the fitness function when constraints are violated.

$$f_1(\mathbf{x}) = \phi_1(\mathbf{x}) \quad (51)$$

$$f_1(\mathbf{x}) = \phi_1(\mathbf{x}) + \left(\sum_{j=1}^6 c_j \max[0, g_j(\mathbf{x})] \right)_{small} \quad (52)$$

$$f_2(\mathbf{x}) = \phi_2(\mathbf{x}) + \left(\sum_{j=1}^6 c_j \max[0, g_j(\mathbf{x})] \right)_{medium} \quad (53)$$

$$f_3(\mathbf{x}) = \phi_3(\mathbf{x}) + \left(\sum_{j=1}^6 c_j \max[0, g_j(\mathbf{x})] \right)_{large} \quad (54)$$

The N -Branch Tournament Selection GA was run several times to assess the repeatability of the results of the algorithm. This multiobjective GA was able to find 24 Pareto optimal points that are feasible and non-dominated with respect to the four objectives described in Equation 51 through 54. The Pareto optimal set of solutions are described in the following section. Additionally, a single objective GA was used to design each of the three satellites under consideration in separate runs. The results of these three single objective GA runs are compared to the results of the multiobjective GA run to assess the effect designing for common architectures on the performance of the individual satellites.

ANALYSIS OF THE SPACECRAFT PLATFORMING OPTIMIZATION RESULTS

The Pareto front includes 24 points; each point represents a product line that is composed of three satellite configurations with three payload sizes catering to three different market segments. The Pareto set was obtained on average in 75 generations corresponding to 37,392 function evaluations [(75+0th generation) × population size (4×123)] and about 15 minutes of run time on a Pentium 4 processor using serial processing. The 24 points on the Pareto front are shown in Figure 6; this is a non-traditional Pareto front because four different objectives are all included in this two-dimensional plot.

The horizontal axis in Figure 6 represents the value of the first objective, which is the number of common technology choices among all three satellites. A maximum of 13 common technology choices can be achieved. There are five levels of commonalities on the Pareto front that are shown in Figure 6; these optimal numbers of common technology choices range from a minimum of nine to a maximum of 13. The vertical axis represents the aggregate launch mass of all three satellites in a product line. Although the aggregate launch mass of all three satellites is not one of the objective functions (the true objectives are the individual launch mass for each satellite), the aggregate mass is used in Figure 6 to allow the reader to visualize the Pareto front (hyper-surface) with all its four objectives. Some of the points in Figure 6 are numbered and labeled with the launch mass values of each of the three satellite configurations that are represented by the point. Those points are used in the analysis of the Pareto front.

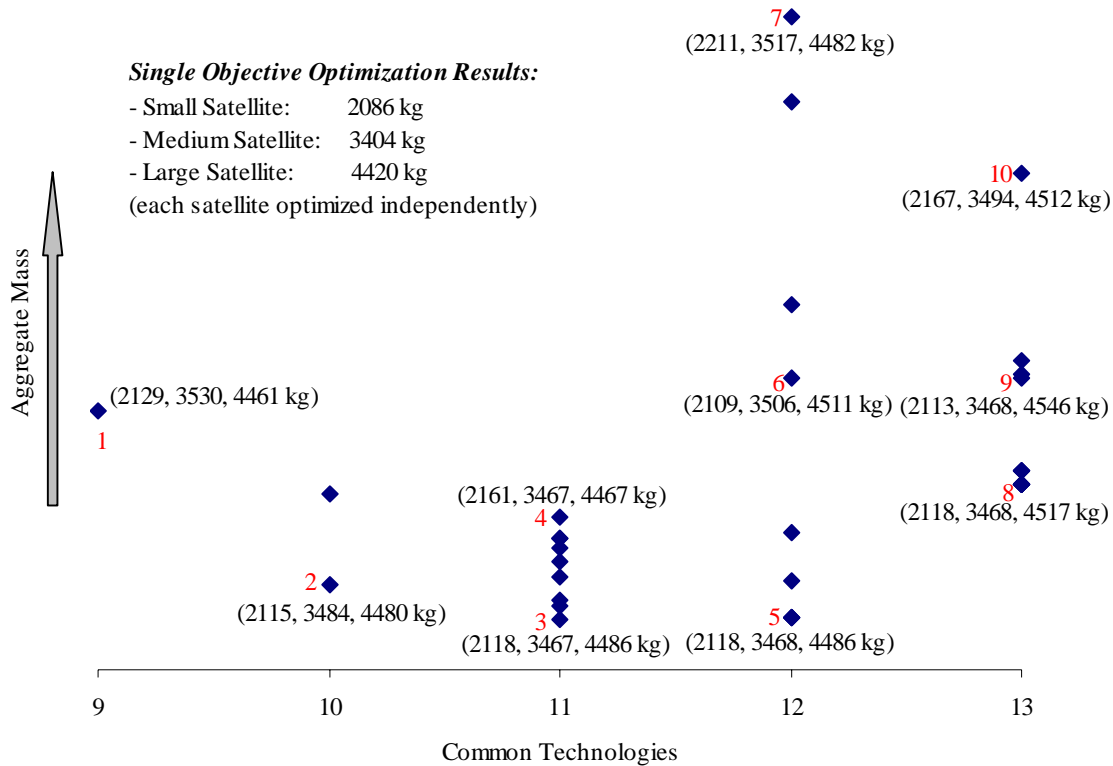


Figure 6: Pareto Front for a three unit satellite product line.

The issue of non-dominance, or non-inferiority, in the Pareto front can be illustrated by investigating the product line architectures represented by single points in Figure 6. Every point (product line architecture) in this Pareto front is a non-dominated point. Compare, for example, product lines that have the same level of commonalities. Both Points 3 and 4 have 11 commonalities and the same configuration for the medium size satellite (3467 kg); however, Point 3 has a heavier configuration for the large satellite (4486 kg) and Point 4 has a heavier configuration for the small satellite (2161). Now, compare two product lines on the Pareto front with different commonality levels. Points 5 and 8 have the same small and medium size configurations (2118 and 3468 kg respectively); however, Point 5 has fewer commonalities and Point 8 has a heavier configuration for the large satellite. These two examples illustrate the non-dominance characteristics of the discrete points or product line architectures on the Pareto front.

The results of the single-objective GA runs that optimize the three satellites independently, i.e. without consideration to commonalities of technology choices,

are summarized at the upper left corner of Figure 6. The GA runs for the optimization of the small, medium and large satellites converged on average in 57, 49 and 50 generations respectively, which correspond to 9512, 8200, and 8364 function evaluations respectively. Here, the function evaluations are computed as the product of number of generations (the 0th generation is added) and the population size. The population size is taken as four times the chromosome length (41 bits for single objective optimization runs), which is typical in GA problems formulation. It is noticed that the sum of the computational effort of the three single-objective GA runs is 70% of the computational effort of the multiobjective GA run. These results show that the *N*-Branch Tournament Selection GA does not require much computational effort beyond what is required by a single-objective GA in the product family design problem.

Figure 6 shows that the Pareto front does not exhibit a wide range of satellite configurations, and does not show a vast tension between the commonality objective and the individual satellite launch mass objectives. For example, the largest satellite has a

minimum launch mass of 4461 kg (Point 1) and shares nine technology choices with the other two satellites. This large satellite has a maximum launch mass of 4517 kg (Point 8) with a configuration that shares the maximum allowable 13 technology choices with the other two small and medium satellites. The difference in launch mass values between these two extreme points on the Pareto front (anchor points) for the large satellite available configurations is only 56 kg. This little extra mass can be easily accommodated in the design of the large satellite because the benefit of a maximum commonality level is more valuable. Furthermore, this largest configuration of the large satellite (Point 8) is only 97 kg heavier than the optimal satellite configuration (4420 kg) when it is optimized independently using its launch mass as a single objective function.

The lack of variability in satellite configurations in the Pareto front, hence the lack of tension between the objectives, is due to the limitation imposed by the satellite performance estimation models on the analysis. The models implemented in this work were specifically developed for use with medium size satellites. However these models were used in this work to estimate the performance of small and large satellites because there were no other better models that are publicly available and could be used in the analysis. Future work will aim at developing high fidelity models that can accurately estimate the performance of multiple satellite sizes. These models will be incorporated within the successful framework that this paper has established for the optimization of communication satellites product families.

CONCLUSIONS

This paper presents an optimization-based framework that incorporates product family concepts in the concurrent design of multiple geosynchronous communication satellites with variable payload requirements catering to multiple market segments. The suggested framework integrates multiobjective optimization approaches with system level satellite performance estimation models to generate optimal product line architectures with maximum common technology choices that are shared by all satellites in the product family, and with minimum launch mass satellite configurations. The multiobjective approach generates a Pareto optimal set of product line architectures that resolve the tension between the maximum technology choices commonality objective and the independent satellites' optimal performance objectives. The Pareto optimal set of product line

architectures can help systems engineers and decision makers identify major tradeoffs and evaluate several product line concepts across all the design objectives. The approach also enforces design constraints, and filters the solutions for feasibility to ensure that all designs included in the approximate Pareto set are feasible designs. Providing this type of information about the satellite product line design space should reduce both the time and the cost of the conceptual design phase.

The horizontal platform leveraging strategy that is employed in this research allows components and subsystems from products serving different market segments to be shared among all the satellites in a product family. The main benefits of this strategy are the flexibility it provides to manufactures and the potential cost reductions associated with sharing of R&D, development and manufacturing costs, which can all lead to market dominance and maximum profit margins.

REFERENCES

- ¹ Hassan, R., *Genetic Algorithm Approaches for Conceptual Design of Spacecraft Systems Including Multiobjective Optimization and Design under Uncertainty*, doctoral thesis, Purdue University, May 2004.
- ² Hassan, R., and Crossley, W., "Multiobjective Optimization of Communication Satellites with a Two-Branch Tournament Genetic Algorithm," *Journal of Spacecraft & Rockets*, Vol. 40, No. 2, 2003, pp. 266-272.
- ³ Hassan, R., and Crossley, W., "Variable Population-Based Sampling for Probabilistic Design Optimization with a Genetic Algorithm," AIAA-2004-0452, *42nd Aerospace Sciences Meeting*, Reno, NV, January 2004.
- ⁴ de Weck O., Suh E. S., Chang D., "Product Family and Platform Portfolio Optimization", DETC03/DAC-48721, *Proceedings of DETC'03 2003 ASME Design Engineering Technical Conferences*, Chicago, IL, Sept. 2-6, 2003.
- ⁵ Willcox, K., and Wakayama, S., "Simultaneous Optimization of a Multiple-Aircraft Family," *J. of Aircraft*, Vol. 40, No. 4, July–August 2003, pp. 616-622.
- ⁶ Simpson, T., and D'Souza, B., "Assessing Variable Levels of Platform Commonality within a Product Family Using a Multiobjective Genetic Algorithm," AIAA 2002-542, *Proceedings of the 9th AIAA/ISSMO*

Symposium on Multidisciplinary Analysis and Optimization, Atlanta, Georgia, 4-6 September 2002.

⁷ Gonzalez-Zugasti, J., Otto, K., and Baker, J., "A method for Architecting Product Platforms," *Research in Engineering Design*, Vol. 12, 2002, pp. 61-72.

⁸ Caffrey, R., Simpson, T., Henderson, R. and Crawley, E., "The Strategic Issues with Implementing Open Avionics Platforms for Spacecraft," IEEE-434-02, *IEEE Aerospace Conference*, Big Sky, 2002.

⁹ Caffrey, R., Simpson, T., Henderson, R. and Crawley, E., "The Economic Issues with Implementing Open Avionics Platforms for Spacecraft," AIAA-2002-1870, *20th AIAA International Communications Satellite Systems Conference and Exhibit*, Montreal, Quebec, Canada, 2002.

¹⁰ Caffrey, R., Simpson, T., Henderson, R. and Crawley, E., "The Technical Issues with Implementing Open Avionics Platforms for Spacecraft," AIAA-2002-0319, *40th AIAA Aerospace Sciences Meeting and Exhibit*, Reno, NV, 2002.

¹¹ Meyer H. and Lehnerd A., *The Power of Product Platform: Building Value and Leadership*, The Free Press, 1997.

¹² Goldberg, D., *Genetic Algorithms in Search, Optimization and Machine Learning*, 1st ed., Addison-Wesley, MA, 1989, pp. 19-63.

¹³ Pareto, V., "General Notion of Economic Equilibrium," *Manuale di Economia Poltica*, Societa Editrice Libreria, Milan, Italy, 1906 (translated to English by A. S. Schwier, *Manual of Political Economy*, MacMillan, NY, 1971), pp. 103-180.

¹⁴ Crossley, W., Cook, A., Fanjoy, D., and Venkayya, V., "Using the Two-Branch Tournament Genetic Algorithm for Multiobjective Design," *AIAA Journal*, Vol. 37, No. 2, Feb 1999, pp. 261-267.

¹⁵ D'Souza, B., and Simpson, T., "A Genetic Algorithm Based Method for Product Family Design Optimization," *Engineering Optimization*, Vol. 35, No. 1, 2003, pp. 1-18.

¹⁶ Wertz, J., and Larson, W., ed., *Space Mission Analysis and Design*, Microcosm Press, Torrance, CA, 1999, pp. 241-497.

¹⁷ Ashley, S. "Bringing Launch Costs down to Earth," *Mechanical Engineering*, Vol. 120, No. 10, 1998, pp. 62-68.

¹⁸ Mugnier, D., "ARIANE 4 User's Manual," Issue No. 2, [www http://www.arianespace.com/docs_manual.html], Feb. 1999.

¹⁹ Timmins, A., "A Study of Total Space Life Performance of GSFC Spacecraft," NASA-TN-D-8017, MD, July, 1970.

²⁰ Strauss, R., "Reliability of SSPA's and TWTA's," *IEEE Transactions on Electron Devices*, Vol. 41, No. 4, 1994, pp. 625-626.

²¹ Hecht, H., "Reliability Considerations," *Reducing Space Mission Cost*, Wertz, J., and Larson, W. (editors), 1st ed., Microcosm Press, CA, 1996, pp. 285-300.

²² Parkinson, R., "The Hidden Costs of Reliability and Failure in Launch Systems," *Acta Astronautica*, Vol. 44, No. 7, 1999, pp. 419-424.

²³ Isakowitz, S., Hopkins, J. P., and Hopkins, J. B., *International Reference Guide to Space Launch Systems*, 3rd ed., AIAA, VA, 1999, pp. 1-15.